FINITE ELEMENT MODELLING OF THE COMPOSITE ACTION BETWEEN HOLLOWCORE SLABS AND THE TOPPING CONCRETE

Aiham Adawi[1], Maged A. Youssef[1], Mohamed E. Meshaly[2]

[1] Department of Civil and Environmental Engineering, Western University, London, Ontario, Canada, N6A 5B9
[2]Department of Structural Engineering, Alexandria University, Alexandria, Egypt

ABSTRACT

The ultimate strength of hollowcore slabs is greatly affected by their post-cracking behaviour. The composite action between the concrete topping and the hollowcore slab adds another level of nonlinearity. This paper presents a comprehensive finite element study to evaluate the non-linear properties of the interface between a hollowcore slab and its concrete topping. The presented finite element modeling procedure was validated using data from a previous comprehensive experimental study by the authors. The nonlinear material behaviour of the concrete and the prestressing strands were also accounted for. The paper presents a modeling method that realistically simulates the staged construction technique of composite hollowcore slabs. Finite element results allowed understanding changes to the interface properties due to the confining effect of the applied load as well as the interaction between the shear and peel stresses.

Keywords: hollowcore slabs, composite behaviour, interfacial shear and peel stress, nonlinear finite element analysis.

1. INTRODUCTION

Hollowcore slabs are precast/prestressed structural concrete elements that are used in many structures including large occupancy residential and commercial buildings. They are favored over cast-in-place slabs because of their guaranteed quality, ease of installation, and reduced construction times. Variations in the initial prestressing camber for slabs of a given floor result in surface irregularities. To achieve a flat surface finish, a 50 mm concrete topping is commonly cast on top of the hollowcore slabs. If the composite action between the concrete topping and the slab is considered, the load carrying capacity of the floor increases. This requires roughening of the surface of the hollowcore slab to an amplitude of 6.35 mm or 5.00 mm according to ACI 318-08 (2008) and CSA A23.3-04 (2004), respectively. Design engineers may also require the use of bonding agents in addition to the roughening mentioned in the design standards. Such requirements induce additional costs that hollowcore slab manufacturers are keen to avoid. There is also a general consensus among manufacturers that the bond between hollowcore slabs with machine-cast surface and topping concrete is sufficient to develop adequate composite action.

Adawi et al. (2015) presented a comprehensive experimental study on the performance of composite hollowcore slabs. The slab specimens had machine-cast and lightly-roughened surface finishes. The study provided initial evidence that the average interfacial shear strength reaches values higher than the values specified in North American design codes. The analytical linear closed-form solution developed by Adawi et al (2014) showed that interfacial shear stresses in composite hollowcore slabs are not uniformly distributed along the interface. The behaviour of the concrete material becomes highly nonlinear after cracking, which greatly affects its overall response. Therefore, it is necessary to investigate the post-cracking behaviour of composite hollowcore slabs.

The abundant literature on composite action of flexural elements is related to composite steel beams (Fabbrocino et al., 1999; Brozzetti, 2000; Nie et al., 2004; Jurkiewiez, 2009; Liang et al., 2005). In such composite beams, the concrete topping is attached to the top flange of the steel beam using shear connectors (shear studs). Salari et al. (1998) and Queiroz et al. (2006) modeled the shear connectors using spring elements. The force-displacement relationship of those springs was evaluated through push-off tests (Ollgard et al., 1971). A different type of composite steel beams utilizes an adhesive compound to attach the concrete topping to the steel beam in lieu of shear studs. Luo et al. (2012) conducted push-off tests on the bonded composite steel samples to evaluate the shear behaviour of the adhesive. A nonlinear Finite Element Analysis (FEA) was also performed to simulate those tests. The FEA model was then extended to model full-scale composite beams and its results were validated using the experiments by Bouazaoui et al. (2007).

Celal (2011) studied the shear capacity of non-composite hollowcore slabs using 3-D nonlinear FEA. Solid elements were used to model concrete and 3-D truss elements were utilized for the strands. The bond between the strands and the surrounding concrete was simulated used bond-slip relationships and implemented in the model using nonlinear spring elements. The FEA results were validated using full scale experimental test results. Wu (2015) carried out 3-D nonlinear FEA on hollowcore slabs with FRP sheets attached to their webs. The FRP sheets were modeled using shell elements. To the authors' knowledge, there is a lack of research addressing modeling of composite hollowcore slabs. Mones (2012) conducted multiple push-off tests on composite hollowcore slabs with different surface finishes. Mones also modeled the composite behaviour of hollowcore slabs using 2-D plane-stress elements. Spring elements resembled the interfacial shear stress. The analysis assumed linear-elastic behaviour, did not account for the peel behaviour, did not account for the staged construction procedure, and was not validated.

This paper summarizes the push-off and full-scale tests that were conducted by the authors at Western University, Canada (Adawi et al., 2015). The tests resemble the actual state of stresses at the interface that involves both shear and peel stresses. FEA modeling of the push-off tests was then conducted to determine the interfacial shear and peel constitutive relationships for each slab. These relationships were then used to model the full-scale tests. The actual shear stress distribution along the interface between hollowcore slabs and the concrete topping was then evaluated.

2. PUSH-OFF AND FULL-SCALE TESTS

The push-off tests were conducted to evaluate the shear and peel stiffnesses as well as the shear strength of the interface layer. The tested hollowcore slabs had a thickness of 203 mm, a surface area of 1220 mm by 1220 mm and a concrete compressive strength of 41 MPa. The concrete topping had a surface area of 508 mm by 508 mm, a thickness of 50 mm, and a concrete compressive strength of 32 MPa. A total of seven slabs (SMA1-2, SRA1-1, SRA1-3, SRB1-1, SRB1-2, PSMA4-2, and PSMA4-3) were tested. “M” and “R” refer to the surface finish of the slab as either machine-cast or lightly-roughened, respectively. “A” and “B” refer to the slab manufacturer.

Push-off tests were conducted in the vertical orientation. The concrete topping was resting on a steel plate, and a downward force was applied to the hollowcore slab. Two steel beams were positioned on the back of the hollowcore slab to provide stability. The concrete topping was instrumented with five strain gauges (S1 to S5), two peel displacement gauges (L1 and L2), and two slip displacement gauges (L3 and L4). The push-off test setup and instrumentation are shown in Fig. 1. The displacement and strain readings obtained from L1 to L4 and S1 to S5 are provided in Adawi et al. (2015). The tests were conducted by applying the load using the MTS actuator at a rate of 10 kN per minute until full separation between the hollowcore slab and the concrete topping occurred.

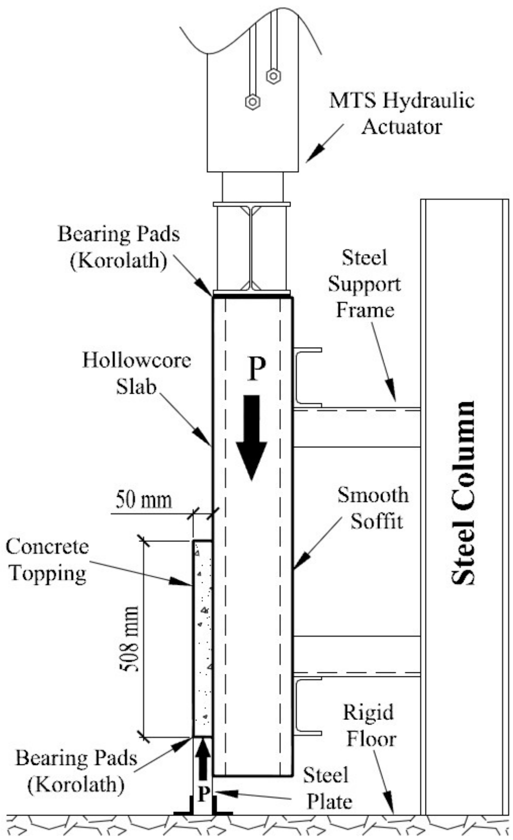

(a) Elevation view.

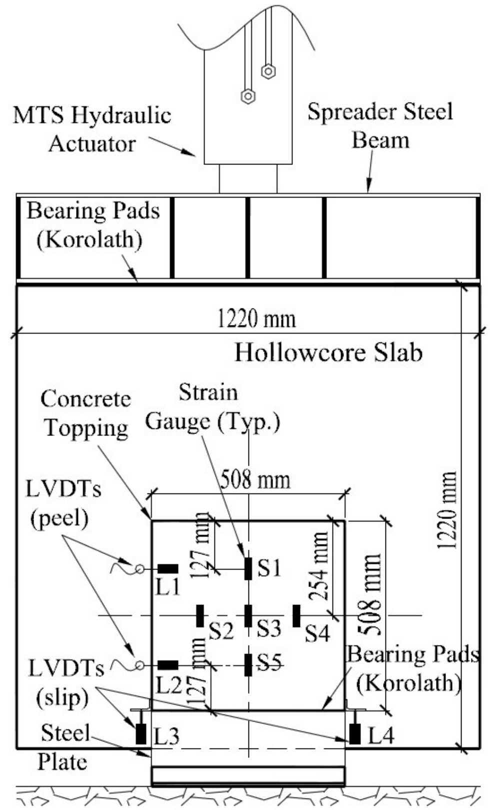

(b) Side view.

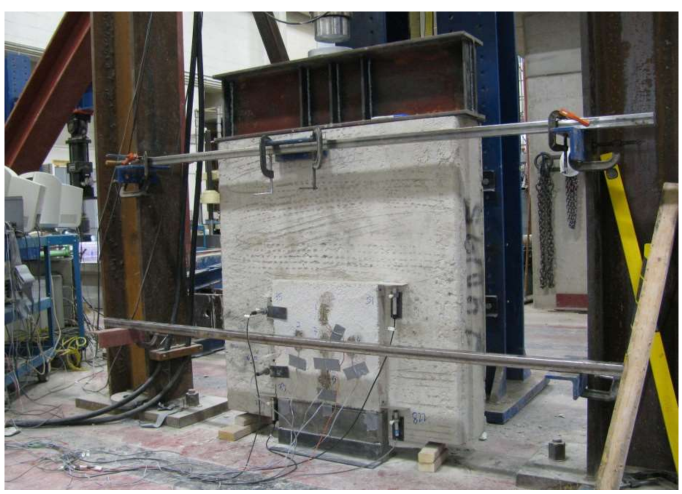

(c) Test photo.

Fig. 1: Push-off test setup and instrumentation (Adawi et al., 2015).

Full-scale tests were then conducted to understand the behaviour of the interface in typical hollowcore applications. Table 1 provides details about the full-scale tests. While five of the slabs (FMA2-1, FMA2-2C, FMB2-1C, FMB2-2, and FMB2-3) had machine-cast surface finish, slab FRA2-3 had a lightly-roughened surface finish. The length and width of the slabs were approximately 3658 mm and 1220 mm, respectively. The concrete topping had a thickness of 50 mm and a concrete compressive strength of 30 MPa.

Table 1: Full-scale test slabs

Slab	Concrete Compressive Strength, f'_c, MPa	Thickness, mm	Prestressing Strands
FMA2-1	53	203	4-13 mm
FMA2-2C	50	203	4-13 mm
FRA2-3	51	253	6-13 mm
FMB2-1C	62	203	7-13 mm
FMB2-2	58	203	7-13 mm
FMB2-3	60	203	7- 13 mm

Fig. 2 shows a typical full-scale test. The load (P) was applied at mid-span using a steel spreader beam. The figure also shows the instrumentation for slabs FMA2-1, FRA2-3, FMB2-2, and FMB2-3 that had full concrete topping, and slabs FMA2-2C and FMB2-1C that had discontinuous topping. The vertical deflection was measured at mid-span using displacement gauges: LE and LW. For slabs with full concrete topping, slip was measured using SLE1 & SLE2 at the east side and SLW1 & SLW2 at the west side. Peel deformations were not measured for those slabs. For slabs that had discontinuous topping, slip was measured on both sides of the concrete topping using SLCW and SLCE. Peel deformations were measured using PCW and PCE. Strain gauges were also attached to the hollowcore slabs (SHCE and SHCW) and the concrete topping (STE and STW) at mid-span. The composite slabs were loaded at mid-span at a rate of 10 kN per minute up to failure. More details about the push-off and full-scale tests are given by Adawi et al. (2015).

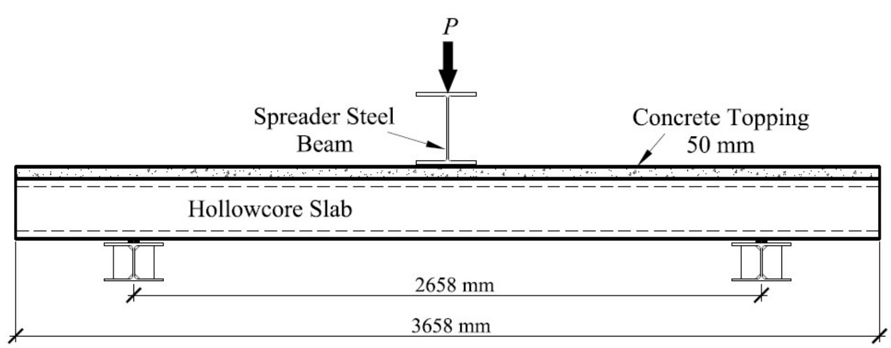

a) Typical full-scale test setup.

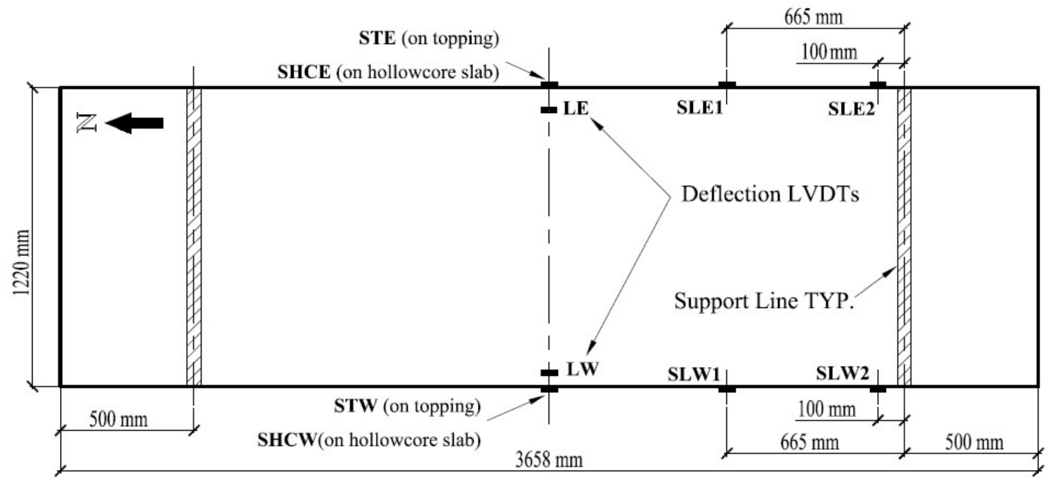

b) Instrumentation of slabs with full concrete topping.

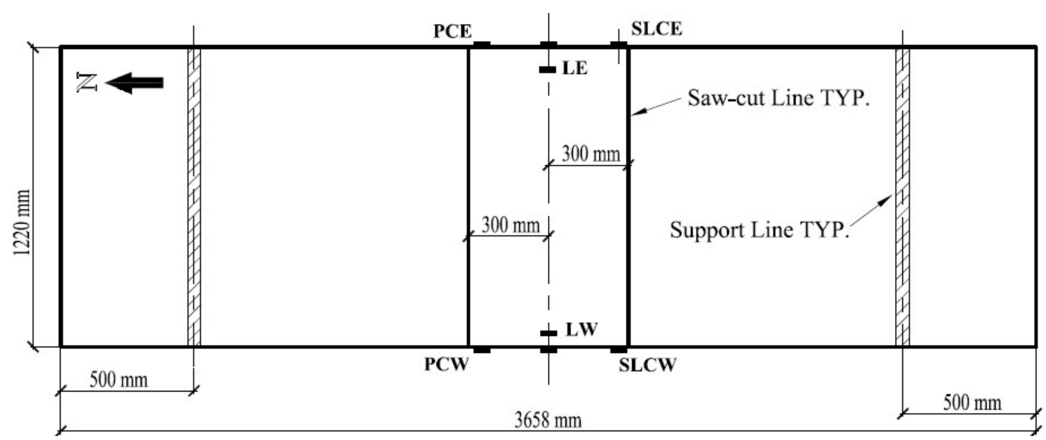

c) Instrumentation of the slabs with discontinuous concrete topping.

(d) Test photo

Fig. 2: Full-scale test setup and instrumentation (Adawi et al., 2015).

3. FINITE ELEMENT MODELING

ANSYS R15.0 (2013) was utilized to model the push-off and the full-scale tests. This section explains the modeling technique including modeling of the prestressing force and the staged construction process. The material models used in the analysis are also presented.

3.1 Push-off Tests

The FEA idealization of the push-off tests is illustrated in Fig. 3. The concrete and the hollowcore slab were modeled using 4-noded plane stress elements (PLANE182) that has two translation degrees of freedom per node. An element size of 12.7 mm resulted in a total of 40 common nodes along the interface layer. While a finer mesh size did not improve the results, a coarser mesh was not deemed necessary since the processing time was quite reasonable.

Two coincident set of nodes were used at the interface, one for the concrete topping and the other for the hollowcore slab. At every node, two contact elements (COMBIN39) were used to attach the hollowcore slab to the concrete topping in the X and Z directions. COMBIN39 is unidirectional nonlinear spring element with generalized force-displacement relationships that can be defined independently for tension and compression. The springs were divided in two groups: edge springs with a tributary area of 6.35 mm by 508.00 mm and interior springs with a tributary area of 12.70 mm by 508.00 mm. Roller supports were used at the loaded end of the hollowcore slab. The lateral deformation of the hollowcore slab was experimentally prevented using a steel support frame, Fig. 1. This frame was modeled using compression only springs. The load was then applied on the concrete topping in a force controlled manner. The applied load resembles the reaction force of the steel plate as illustrated in Fig. 1(a).

3.2 Full-scale Test

The full-scale tests were conducted using a three-point bending test setup as shown in Fig. 2. The FEA idealization of the test is demonstrated in Fig. 4. Similar to the push-off test, the main components of the full-scale test are: the hollowcore slab, the concrete topping and the interface between the hollowcore slab and the concrete topping. 6-noded and 8-noded 3-D solid elements (SOLID65) were used to model the hollowcore slab and the concrete topping, respectively. The interface layer between the hollowcore slab and the concrete topping was modeled using nonlinear spring elements. A typical 3-D model for the composite hollowcore slab is shown in Fig. 5. The slab could not be modeled using a 2-D model as such a model does not support the features used to account for the staged construction technique (section 3.3.2). The prestressing strands were modeled using 3-D truss elements (LINK180) that have two nodes with three translational degrees of freedom at each node. The coincident nodes at the interface were connected using nonlinear spring elements (COMBIN39).

The geometry of a typical composite hollowcore slab was initially created by using block shapes. Several ANSYS geometry tools including “BOOLEANS” were used to create the voids in the hollowcore slab. The meshing was first conducted on the cross section area using the generic area element (MESH200) as shown in Fig. 6. The meshed cross section was then swept over the entire hollowcore slab using the (SOLID65) concrete element. Aspect ratio adequacy was automatically verified using the ANSYS recommended built-in criteria.

The boundary conditions simulated the actual support conditions of the composite slab in the full-scale test, Fig. 4. The bottom nodes at the hinged end of the slab were restricted in the Z and

Y directions while the nodes at the roller support were only restricted in the Y direction. The load, (P), was applied at the midspan nodes located at the top of the concrete topping. Each strand consisted of a number of LINK180 elements that have the same length as the concrete elements along the Z direction, Fig. 6.

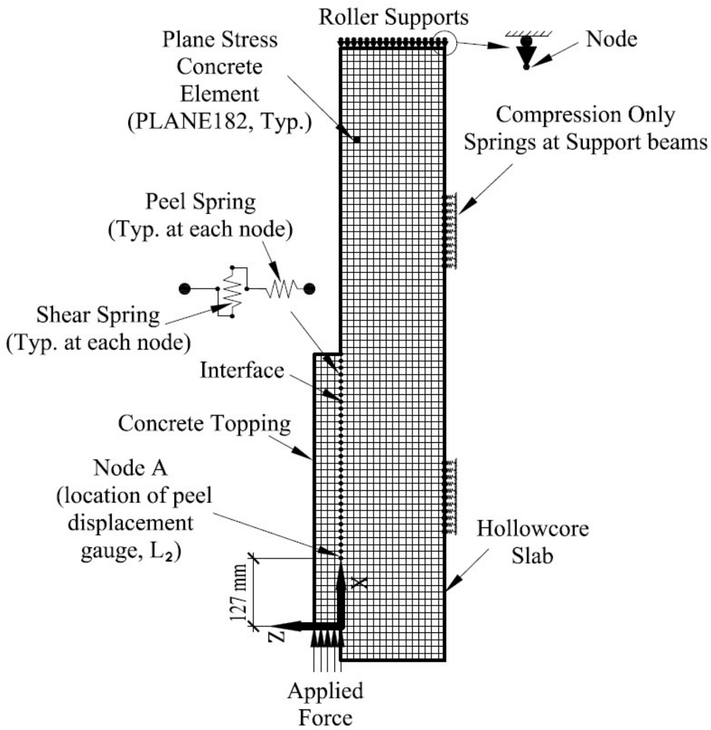

Fig. 3: Finite element idealization of the push-off test.

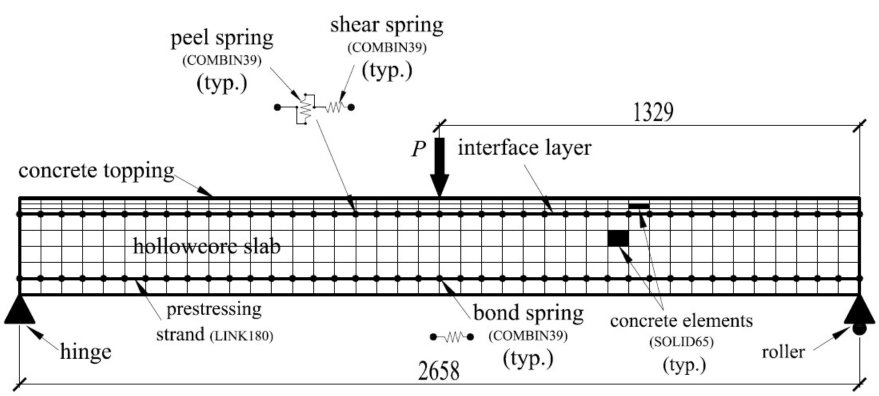

Fig. 4: FE idealization of the full-scale test.

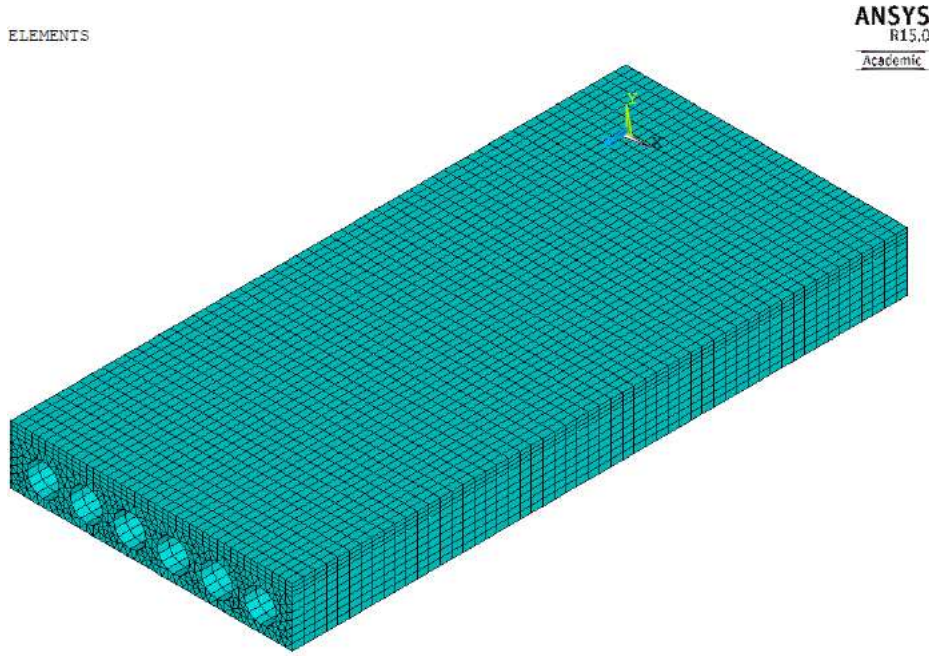

(a) General 3-D view of the modeled composite hollowcore slab.

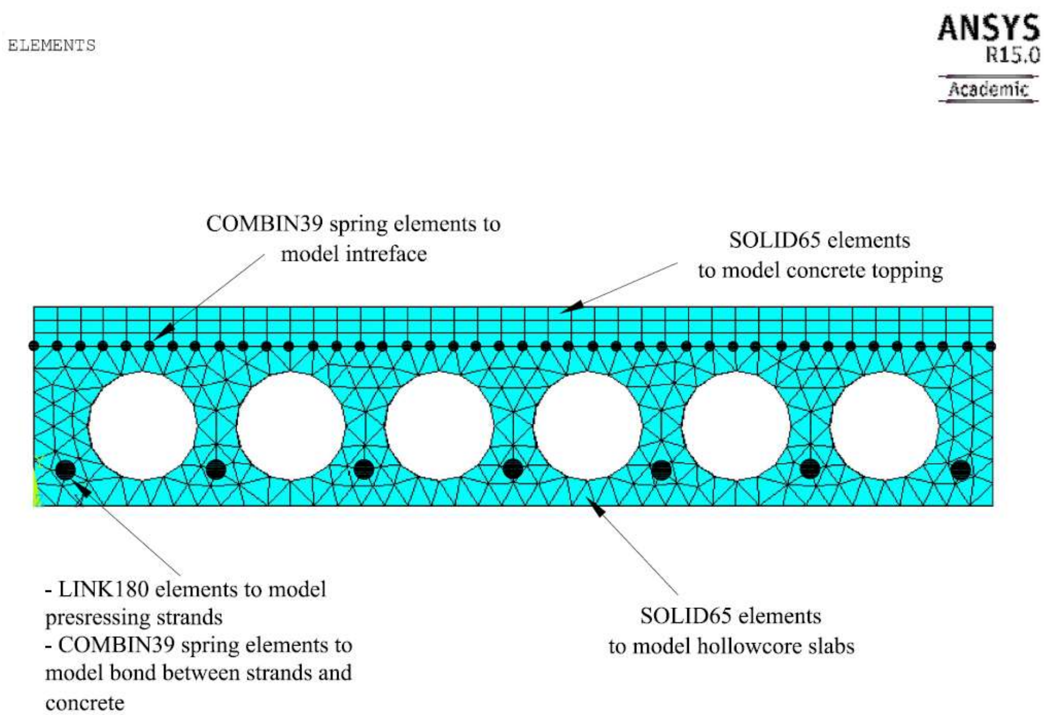

(b) Cross section of the composite slab.

Fig. 5: Finite element model of the full-scale test

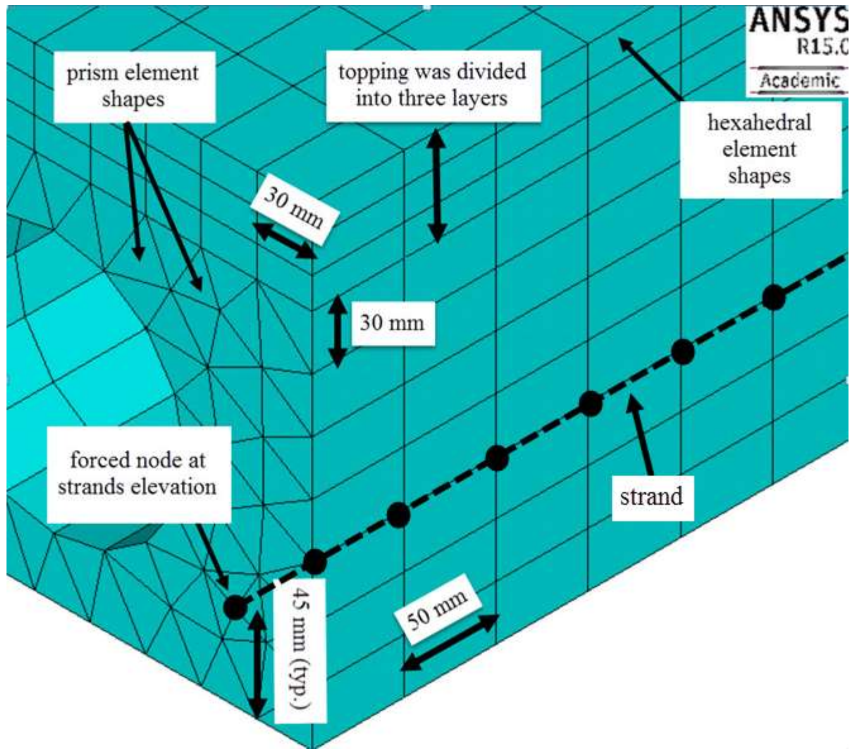

Fig. 6: Meshing layout.

3.3 Special Modeling Techniques

Modeling the composite hollowcore slab involves dealing with two complex issues: the transfer of the prestressing force and the strain discontinuity between the hollowcore slab and the concrete topping. The following sections explain how those two issues were addressed.

3.3.1 Prestressing Force

The jacking stress was 70% of the strand's ultimate tensile strength. Prestress losses due to anchorage slip, relaxation, shrinkage, and creep were estimated to be 15% on the day of testing. The strain in the prestressed strands at the time of testing was 0.0055. This strain was applied using the "initial state" (INISTATE) command. Bond between the hollowcore slab and the prestressing strands was modeled using nonlinear spring elements (COMBIN39), as shown in Fig. 7.

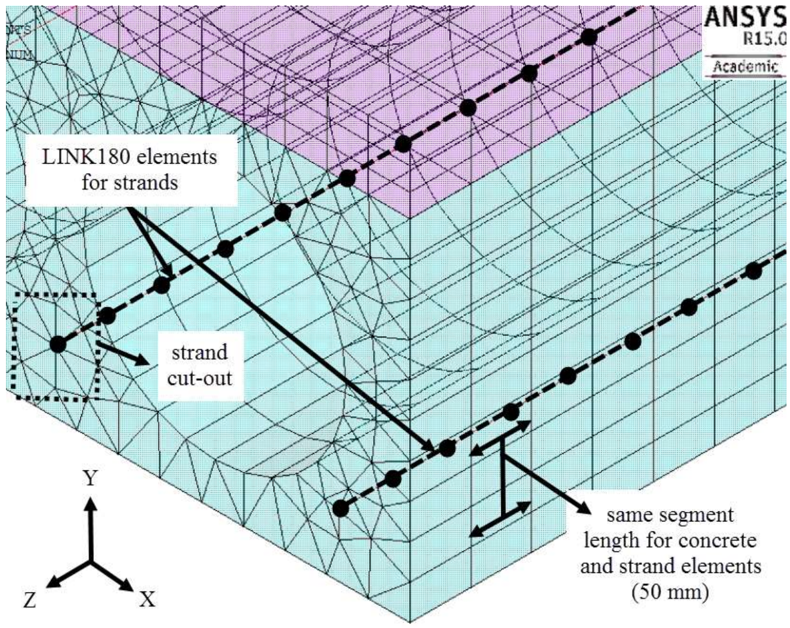

(a) Modeling of strands.

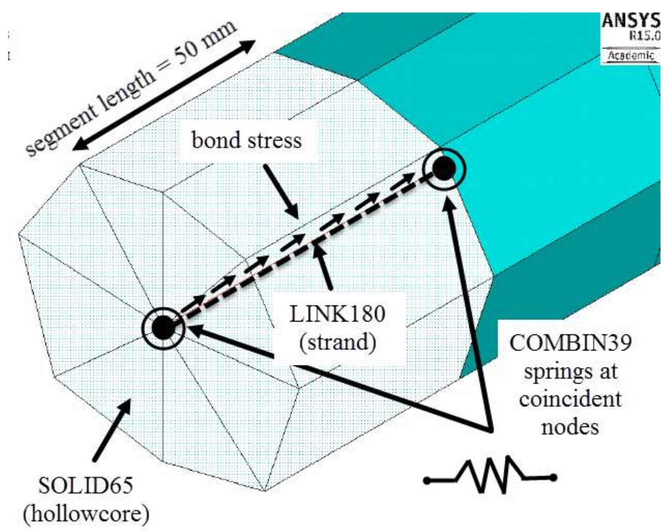

(b) Location of bond springs.

Fig. 7: Illustration of the bond-stress modeling.

The constitutive force-displacement curve for those springs was based on the bond-slip model by Balázs (1992), Eq. (1). The bond stress (τ_b) is multiplied by the cylindrical circumferential area of the strand along the segment length to define the spring force at different slip values.

$$\tau_b = 2.324 \times \sqrt{f'_{ch}}(s)^{1/2} \text{ (MPa)} \quad (1)$$

Where (τ_b) is the bond stress in the direction of slip, (f'_{ch}) is the concrete compressive strength of the hollowcore slab, and (s) is the slip between the strand and the surrounding concrete in millimeters.

3.3.2 Strain Discontinuity

The concrete topping was cast after prestressing the hollowcore slabs. Accordingly, the strains and stresses in the concrete topping were equal to zero before applying the external load (P). The interfacial shear and peel stresses were also equal to zero at that stage. Fig. 8(a) illustrates the staged construction process for composite hollowcore slabs. To model this process, the initial stiffness of the concrete topping was significantly reduced such that it does not contribute to the overall stiffness. This was achieved by using the "KILL" feature in ANSYS. The prestressing force was then applied as an initial strain using the (INISTATE) command. Finally, the stiffness of the concrete topping was activated to reflect its actual value using the "BIRTH" feature. The concrete topping and the interface springs were checked to ensure that they did not experience any stresses before applying the load (P) along the entire width of the composite slab as shown in Fig. 8(b).

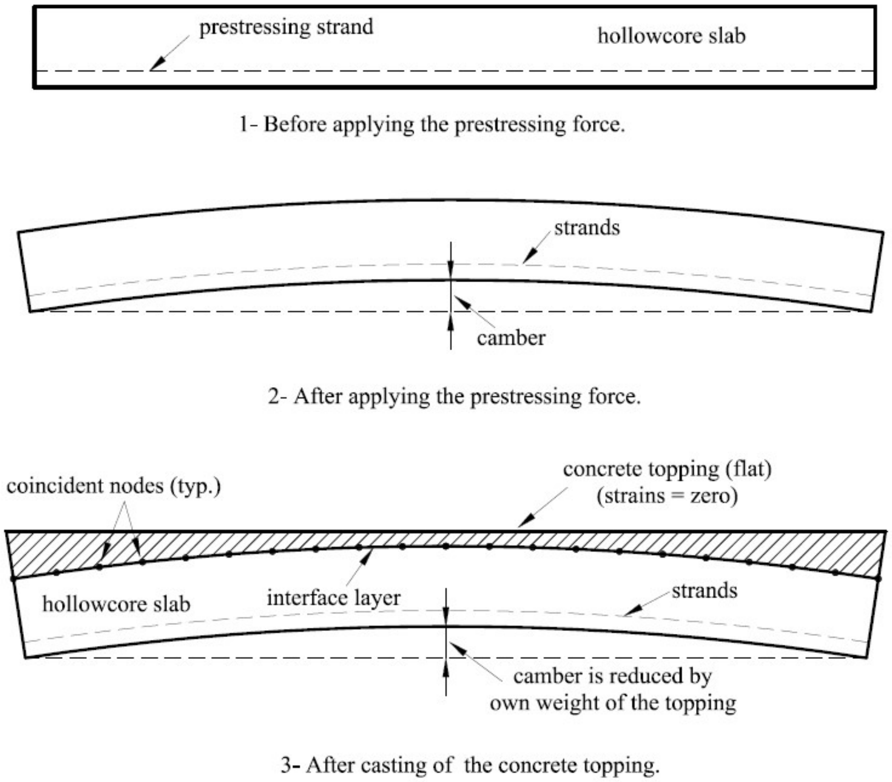

(a) Staged construction steps.

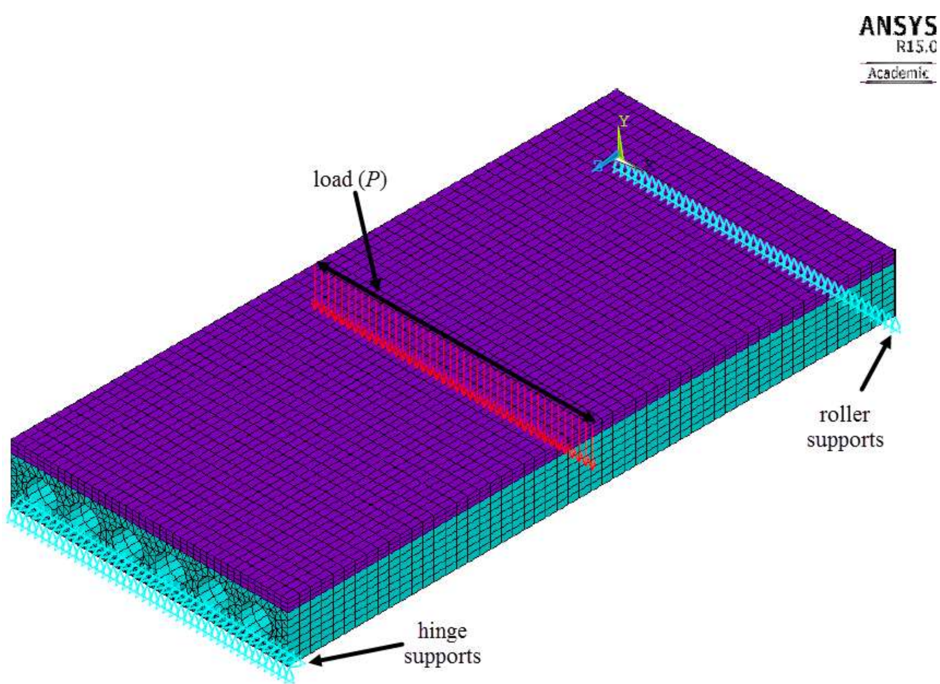

(b) Loaded composite slab

Fig. 8: Strain discontinuity modeling

4. MATERIAL MODELS

4.1 Concrete

The linear isotropic component was defined by the concrete initial tangent stiffness (E_c) that was taken equal to ($3320\sqrt{f'_c}+6900$ MPa) as recommended by Collins (1991). Poisson's ratio was taken equal to 0.2. The unconfined concrete stress-strain relationship Eq. (2), which was proposed by Popovics (1973) and calibrated by Porasz (1989), was used to define the multilinear stage. Shear transfer coefficients were taken as 0.30 and 0.95 for open and closed cracks, respectively (Cheng and Wang, 2010). The uniaxial tensile cracking stress (f_t) was calculated using the formula recommended by Bentz (2000), Eq. (3).

$$f_c = f'_c \frac{n(\varepsilon_c/\varepsilon'_c)}{n-1+(\varepsilon_c/\varepsilon'_c)^{nk}} \text{ (MPa)} \tag{2}$$

$$f_t = 0.45\left(f'_c\right)^{0.4} \tag{3}$$

Where

$$n = 0.8 + \frac{f'_c}{17}$$

$$k = \begin{cases} 1 & (\varepsilon_c/\varepsilon'_c) < 1.0 \\ 0.67 + \dfrac{f'_c}{62} & (\varepsilon_c/\varepsilon'_c) > 1.0 \end{cases}, \quad \varepsilon'_c = \frac{f'_c\, n}{E_c(n-1)}$$

f_c: concrete compressive stress, ε_c: concrete compressive strain, f'_c: peak cylinder compressive strength, ε'_c: strain at peak compressive stress, n: curve fit parameter, k: factor to account for the post peak ductility of high strength concrete.

4.2 Prestressed Reinforcement

The tensile test results of the prestressing strands for slabs from manufacturer A were conducted in accordance with ASTM standard A416/A416M-02 (2002). The ultimate strength (f_{pu}), rupture strain (ε_{pr}), and average modulus of elasticity (E_p) were 1965 MPa, 0.059, and 199,948 MPa, respectively. The tensile test results were not available for strands from manufacturer B, thus, the stress-strain curve for those strands was constructed using the Ramberg-Osgood formulation, Eq. (4), (Collins, 1991).

$$f_p = E_p \varepsilon_p \left\{ A + \frac{1-A}{\left[1+\left(B\varepsilon_p\right)^C\right]^{\frac{1}{C}}} \right\} \leq f_{pu} \tag{4}$$

Where (f_p) and (ε_p) are the stress and strain in the prestressing strand, respectively. The constants A, B and C were taken as 0.025, 118 and 10.0, respectively, as recommended in the 4th edition of the Canadian Precast/Prestressed Institute (CPCI) design manual (2007). The modulus of elasticity (E_p) was taken as 200,000 MPa.

4.3 Failure Criteria

The failure criteria were: (1) maximum principal compressive concrete strain of 0.002 indicating shear failure; (2) longitudinal compressive strain of 0.0035 indicating flexural failure; (3) strands' tensile stress of 1860 MPa or 1965 MPa for the slabs from manufacturers A and B, respectively; (4) force in shear springs reaching their capacity indicating interface shear failure; and (5) force in peel springs reaching their capacity indicating interface peel failure.

5. FINITE ELEMENT ANALYSIS

5.1 Push-off Tests

The assumed force-displacement curve for a typical shear spring is illustrated in Fig. 9(a), which shows three main regions: elastic, inelastic, and failure. In the elastic region, the shear resistance is provided by chemical bond and mechanical friction. The chemical bond is assumed to be lost at the yielding load, (P_{yx}), which corresponds to a sudden change in the stiffness. Sudden failure occurs when the mechanical friction diminishes at a load of (P_{ux}). For the peel springs, Z direction, the resistance is only provided by the chemical bond as shown in Fig. 9(b).

Evaluation of the parameters defining the force-displacement curves for the spring elements involves an iterative procedure. The average load-displacement graph from the push-off tests, P-UX, for slab SRB1-1 is shown in Fig. 10. The P-UX curve was first approximated using multi-linear segments. The linear segments were plotted such that the areas defining the error above and below each segment are equal. The approximated P-UX curve was used to define the initial parameters of the force-displacement curve of the shear springs. By taking into account the number of springs, the following initial parameters were obtained k_{x1}=373.3×10^3 N/mm, k_{x2}=73.4×10^3 N/mm, P_{yx}=2073 N, and P_{ux} =5650 N.

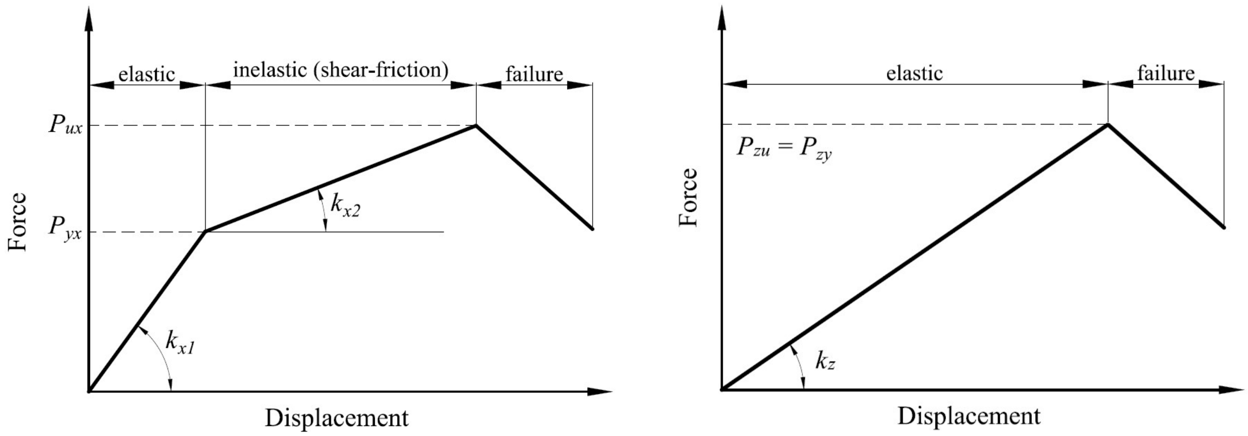

(a) Shear spring. (b) Peel spring.

Fig. 9: Concept force-displacement curves of the interfacial spring elements.

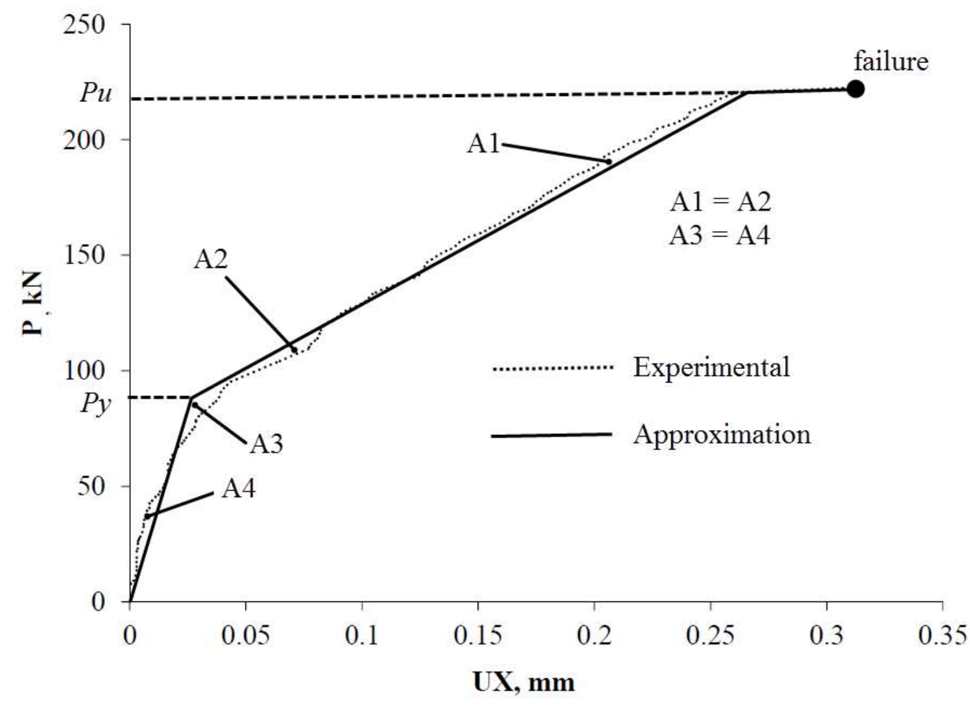

Fig. 10: Approximation of the P-UX graph for slab SRB1-1.

The initial parameters for the peel springs were obtained from the pull-off test results that was presented by Adawi et al. (2015). The bond strength for slab SRB1-1 was estimated to be 1.86

MPa. The tributary area for an interior spring was equal to 6452 mm^2, thus, its maximum tensile force, (P_{yz}), was 12 kN. The peel stiffness, k_z, could not be determined experimentally because of the extremely small displacements. Adawi at al. (2014) provided a closed-form solution of the differential equations governing the push-off tests, which allowed evaluating k_p as 2.1 (N/mm)/mm^2. Accordingly, the stiffness of an interior peel spring, k_z, was equal to 12.9 kN/mm. Peel springs were assumed to have very high stiffness in compression (120 kN/mm) to model the rigid compressive behaviour between the topping concrete the hollowcore slab.

The FEA was conducted in a force-control fashion using automatic load stepping to enhance convergence. The obtained peel and slip deformations were compared to the experimental results. The shear and peel spring stiffnesses were then adjusted based on the FEA results and the analysis was repeated. The iterative process for slab SRB1-1 is illustrated in Fig. 11. The initial properties for the shear and peel springs resulted in slip and peel values that are higher than the experimental results. In addition, it can be observed that the peel response was showing a linear behaviour that is not consistent with the experimental curve. Thus, the stiffness of the shear springs (k_x) was increased in the subsequent trials until a satisfactory match was obtained. A nonlinear force-displacement curve was also used to describe the peel behaviour.

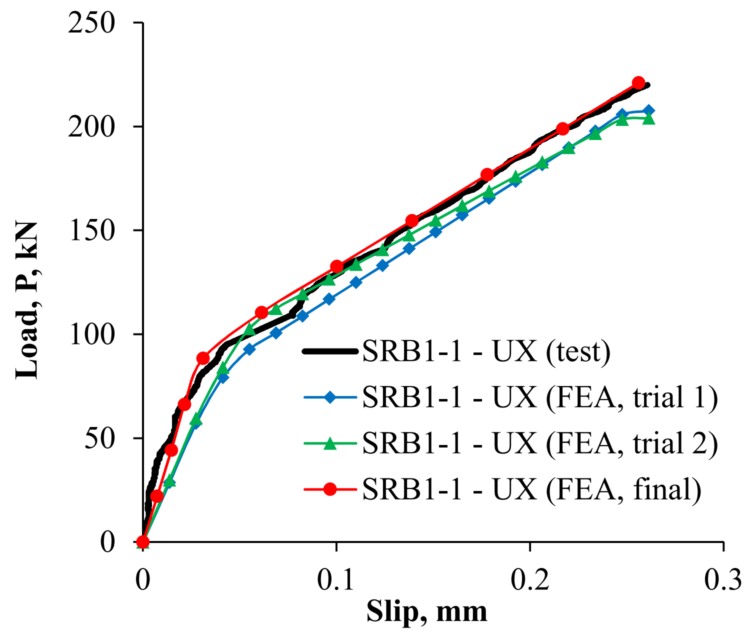

(a) Shear springs.

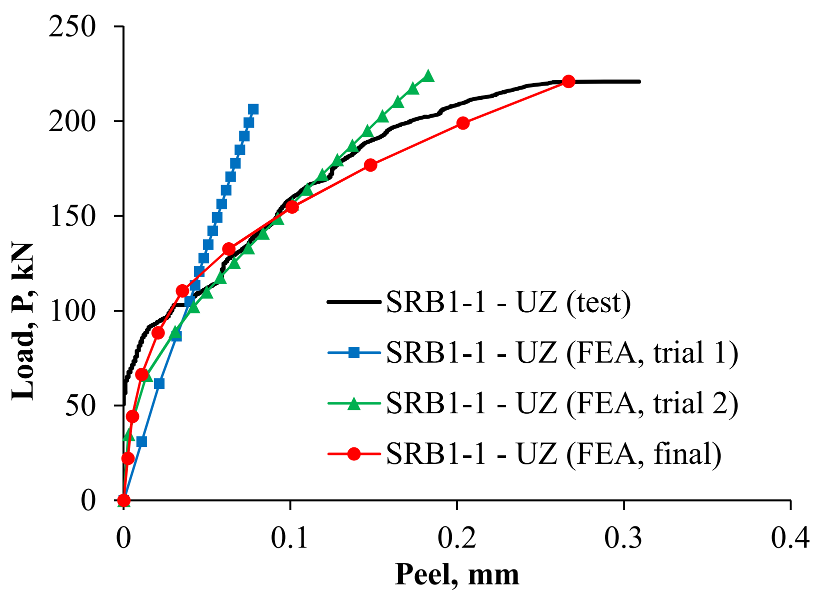

(b) Peel springs.

Fig. 11: Iterations for slab SRB1-1.

The parameters defining the force-displacement curves for the shear and peel springs are summarized in Table 2. Those values govern the nonlinear behaviour of the interfacial shear and peel responses in the push-off tests. The final force-displacement curves for the peel and shear springs are shown in Fig. 12 for slab SRB1-1.

Table 2: Parameters of force-displacement curves of the push-off tests

Slab	Shear Stiffness				Peel Stiffness			
	yield		ultimate		yield		ultimate	
	P_{yx}, kN	k_{x1}, kN/mm	P_{ux}, kN	k_{x2}, kN/mm	P_{yz}, kN	k_{z1}, kN/mm	P_{uz}, kN	k_{z2}, kN/mm
SMA1-2	2.0	333	9.2	12.1	0.45	225	1.15	1.8
SRA1-1	7.0	700	12.7	5.8	1.0	100	1.6	3.2
SRA1-3	8.0	1600	15.0	23.7	1.7	170	2.1	0.8
SRB1-1	2.3	115	6.3	14.3	0.4	20	0.6	0.7
SRB1-2	3.8	38	4.8	12.5	0.6	12	0.75	3.0
PSMA4-2	6.5	650	7.35	6.5	1.3	130	1.35	2.5
PSMA4-3	1.0	200	1.7	0.4	0.15	150	0.19	0.5

Considering slabs from manufacturer (A), k_{x1}, k_{x2}, P_{yx}, P_{ux}, k_{z1}, k_{z2}, P_{uz} and P_{uz} were found to range from: 200 to 650 kN/mm, 0.4 to 12.1 kN/mm, 1.0 to 6.5 kN, 1.7 to 9.2 kN, 130 to 225 kN/mm, 0.5 to 1.8 kN/mm, 0.15 to 1.3 kN and 0.19 to 1.35 kN for the slabs with machine-cast finish and: 700 to 1600 kN/mm, 5.8 to 23.7 kN/mm, 7.0 to 8.0 kN, 12.7 to 15 kN, 100 to 170 kN/mm, 0.8 to 3.2 kN/mm, 1.0 to 1.7 kN and 1.6 to 2.1 kN for lightly-roughened slabs. For lightly-roughened slabs from manufacturer (B), the variables were: 38 to 115 kN/mm, 12.5 to

14.3 kN/mm, 2.3 to 3.8 kN, 4.8 to 6.3 kN, 12 to 20 kN/mm, 0.7 to 3.0 kN/mm, 0.4 to 0.6 kN and 0.7 to 3.0 kN.

The ultimate peel force (P_{zu}) was found to be much less than the peel strength evaluated the pull-off tests, which indicates a reduction in bond strength in the Z direction. This reduction is related to the interaction between the shear and peel stresses along the interface. The peel springs experienced yielding behaviour when the chemical bond between the concrete topping and the hollowcore slab is lost due to shear. A comparison between the linear shear and peel stiffnesses evaluated by Adawi et al. (2014) and the nonlinear stiffnesses evaluated in this paper is provided in Fig. 12 for slab SRB1-1. Fig. 13 compares the strains obtained experimentally and numerically for slab SRB1-1 at failure.

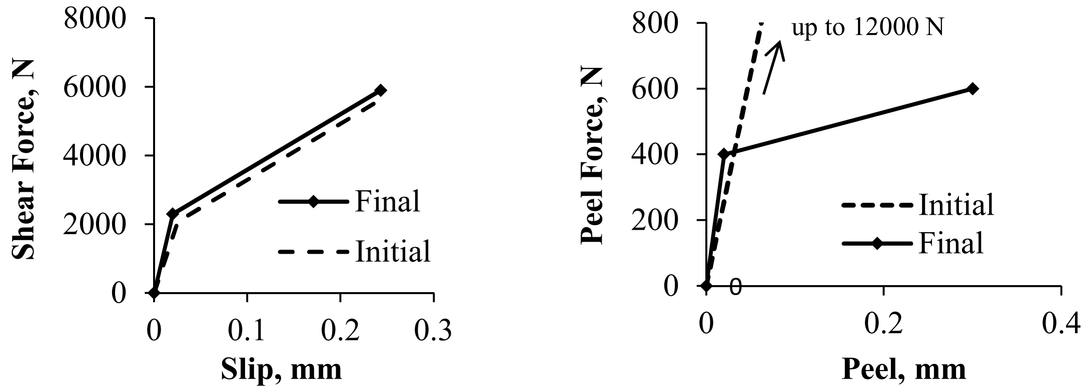

(a): Shear spring (SRB1-1). (b) Peel spring (SRB1-1).

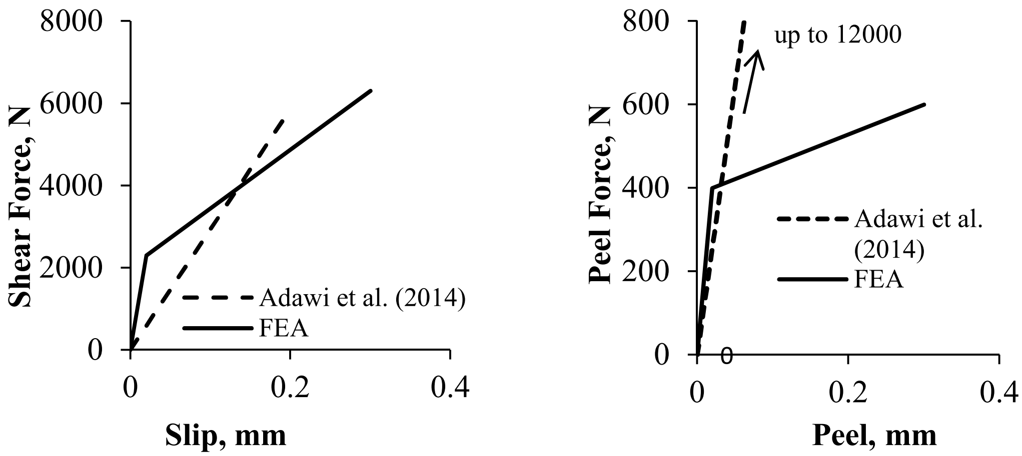

Fig. 12: Interfacial shear and peel springs stiffness for slab SRB1-1

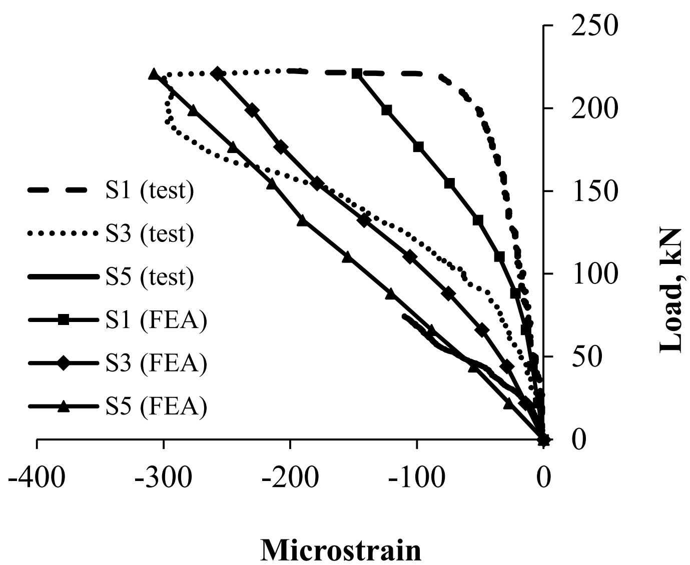

Fig. 13: Strain results for slab SRB1-1

The shear stresses at failure evaluated experimentally, numerically (non-linear FEA), and analytically following the linear model of Adawi et al. (2014) are presented in Table 3. The nonlinear FEA revealed higher shear stresses than the experimental average values. However, they were closer to the average shear stresses as compared to the linear analytical results. The nonlinear shear springs allowed redistribution of the shear stresses, and, thus reduced the value of the maximum shear stress at the loading end. The shear stress distribution along the interface between the concrete topping and the hollowcore slab for SRB1-1 is shown in Fig. 14. Similar behavior was observed for other slabs.

Table 3: Maximum shear stress comparison

Slab	**Maximum shear stress, MPa**		
	Linear Analytical Solution, (Adawi et al., 2014)	**Nonlinear Finite Element Analysis**	**Average Shear Strength (tests),** $v_{h\ avg.}$
SMA1-2	1.69	1.43	1.39
SRA1-1	1.95	1.97	1.95
SRA1-3	2.15	2.33	2.15
SRB1-1	1.24	0.98	0.860
SRB1-2	1.01	0.75	0.710
PSMA4-2	2.47	1.2	1.19
PSMA4-3	0.26	0.26	0.256

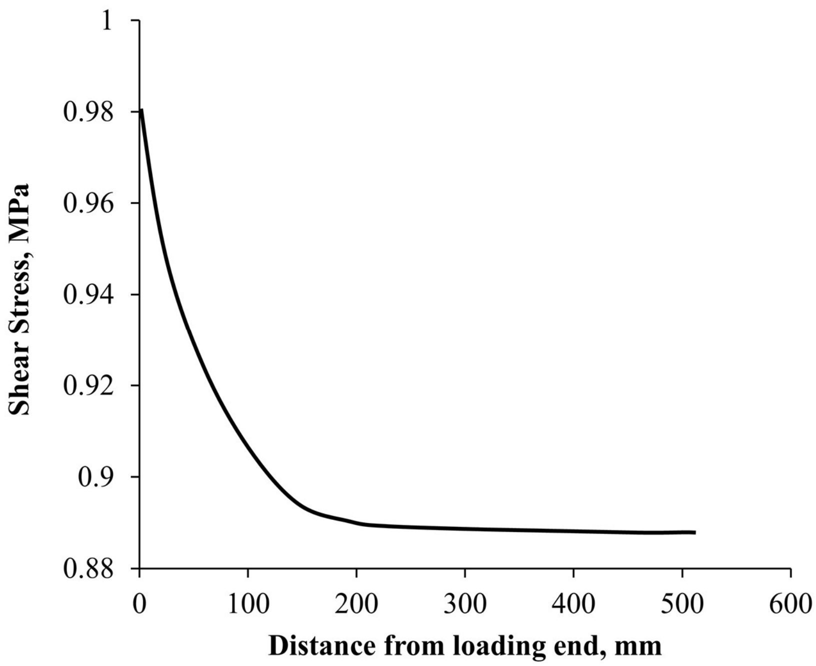

Fig. 14: Interfacial shear stress distribution for slab SRB1-1

5.2 Full-Scale Tests

5.2.1 Load-deflection Response

A summary of the load-deflection results obtained from the experimental tests and the FEA analysis is shown in Table 4. The results are also shown graphically in Fig. 15 for slabs from manufacturer A. It can be noticed that the FEA was fairly successful in capturing the behaviour of the slabs in terms of stiffness and failure load. The ductility was accurately predicted for slabs FRA2-3, FMB2-2 and FMB2-3; which failed in shear. Although the failure mechanism for slab FMA2-1 was accurately predicted as strand rupture, the ductility was underestimated by 30%. Same behaviour was observed for FMB2-1C. Slab FMA2-2C, which had a discontinuous concrete topping, failed by horizontal shear that was followed by concrete compressive strains in the hollowcore slab reaching 0.0035. The difference between the experimental and FEA deflection results is due to the confining effect of the applied load.

Table 4: Load-deflection results

Slab Label	Analysis Type.	Cracking load, kN	Failure load, kN	Deflection at failure, mm	Failure Type
FMA2-1	**Exp.**	157	253	23.1	strands rupture
	FEA	152	257	19.7	
FMA2-2C	**Exp.**	152	244	49.6	interface shear failure then concrete crushing
	FEA	164	206	18.4	
FRA2-3	**Exp.**	275	388	12	flexure-shear failure
	FEA	278	386	11.1	
FMB2-1C	**Exp.**	254	366	26.5	interface shear failure then flexure-shear failure
	FEA	250	376	23	
FMB2-2	**Exp.**	231	410	16.3	flexure-shear failure
	FEA	225	408	15.7	
FMB2-3	**Exp.**	315	512	19.8	flexure-shear failure
	FEA	338	500	16	

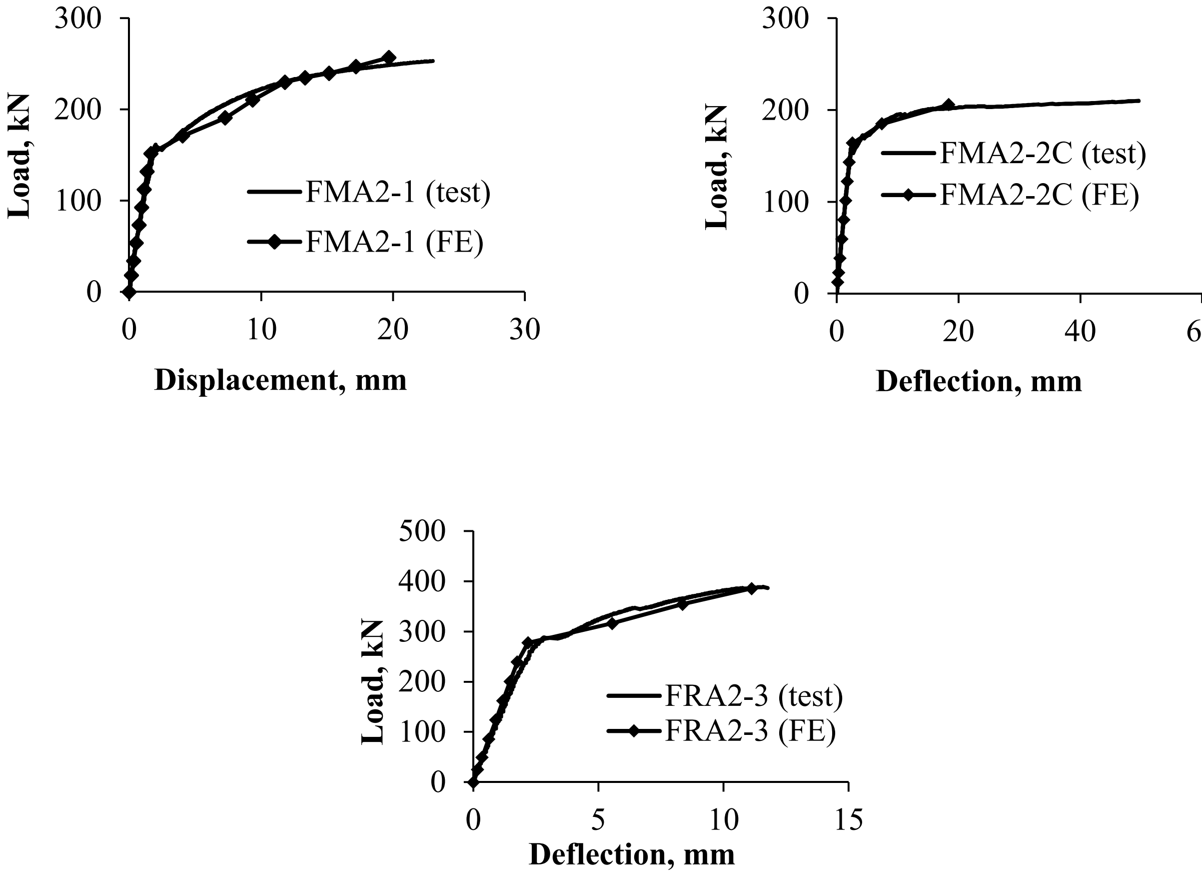

Fig. 15: Load-deflection results for slabs from manufacturer A

5.2.2 Strain Results at the Mid-span Section

The strains for slabs FMA2-1, FMA2-2C, FMB2-1C, FMB2-2, and FMB2-3 show good agreement between the experimental and the FEA results as shown in Fig. 16. The strain relaxation in the concrete topping after cracking was successfully captured in the FEA. The strain distribution along the interface between the hollowcore slab and the concrete topping for slab FMA2-1 is shown in Fig. 17. This distribution is shown at the yielding load (200 kN) for that slab (the load at which the shear stiffness is significantly reduced).

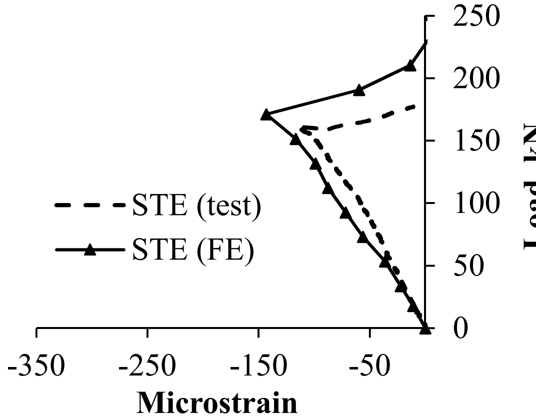

(a) FMA2-1

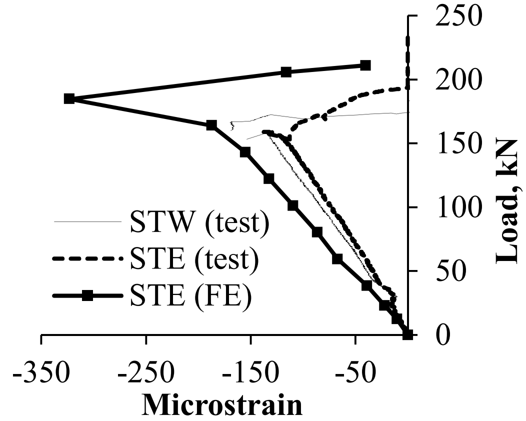

(b) FMA2-2C

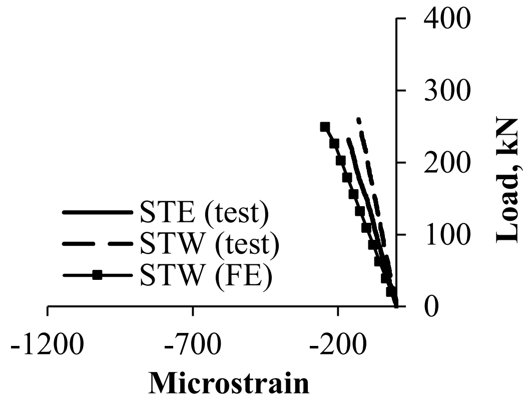

(c) MB2-2C (concrete topping)

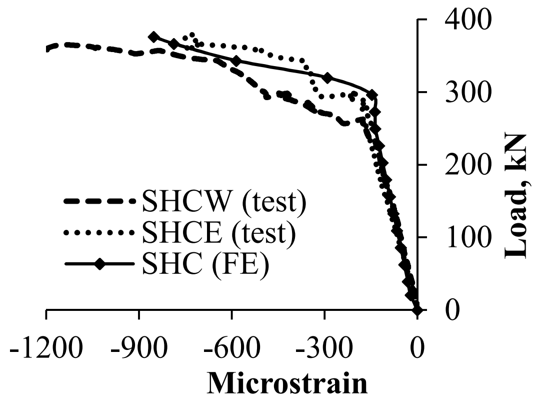

(d) MB2-2C (Hollowcore slab)

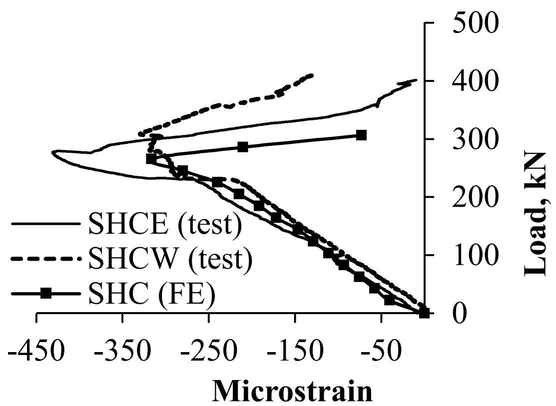

(e) FMB2-2

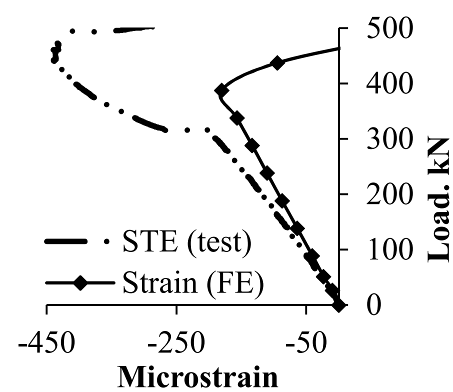

(f) FMB2-3

Fig. 16: Mid-span strain Results

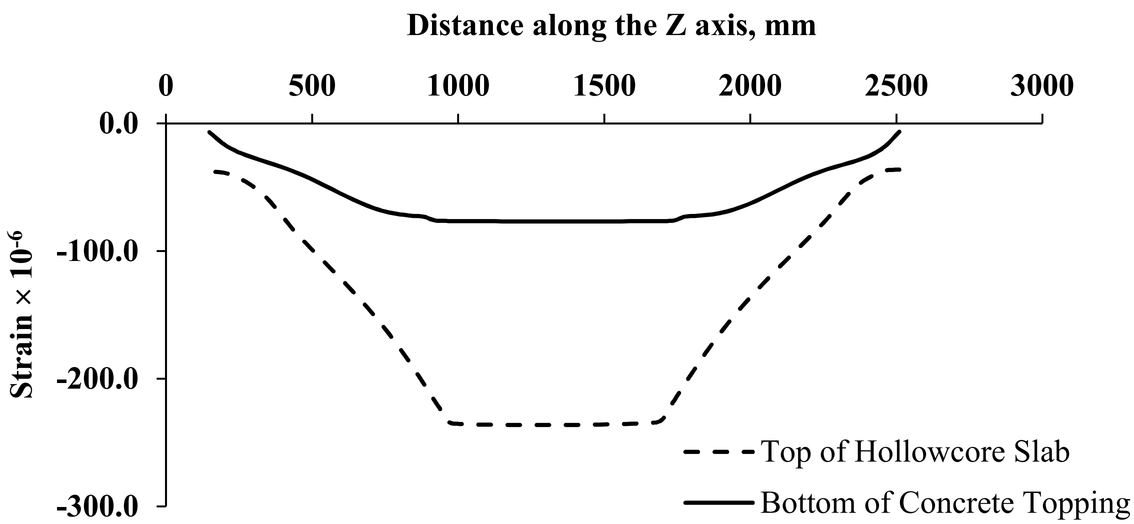

Fig. 17: Strain distribution along the interface at yielding load (200 kN) for slab FMA2-1.

5.2.3 Interfacial Slip and Peel Results

The slip results were compared with the experimental measurements for slab FMB2-2 in Fig. 18. Readings from LVDT SLW2 were found to be in good agreement with the FEA results. Visual inspection of this slab revealed hair cracks in the concrete topping that extended to the interface level and sporadic delamination spots between the concrete topping and the hollowcore slab along the interface (Adawi et al., 2015). This translated in significant slip measured for this slab compared with the rest of slabs that had a full concrete topping.

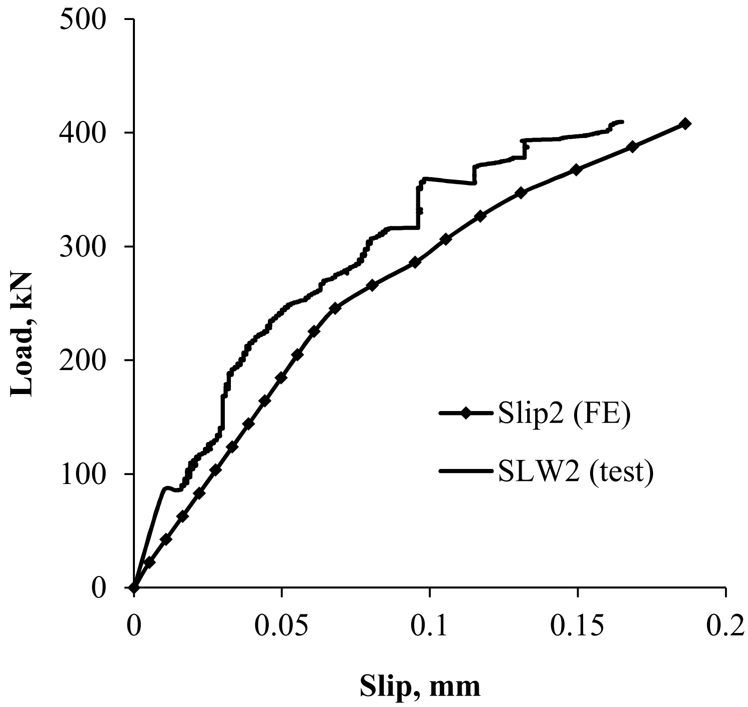

Fig. 18: FEA slip results for slab FMB2-2.

5.2.4 Constitutive Relationships of the Interfacial Springs

The stiffness of the nonlinear springs (COMBIN39) simulating the interface between the hollowcore slab and the concrete topping was crucial in the FEA analysis. The constitutive force-displacement curves were initially based on the FEA results of the push-off tests. The final force-displacement curves were determined using an extensive iteration process to match the full-scale experimental results. The final shear and peel stiffness results along with the parameters defining the force-displacement curves for the interface springs are show in Table 5 and Fig. 19. Difference between these values and the push-off test values can be attributed to the effect of confinement of the interface layer that resulted from the applied load and the interaction between the shear and peel stresses along the interface layer.

Table 5: FEA shear and peel stiffness results for the full-scale test slabs

Slab	**Shear Stiffness**				**Peel Stiffness**			
	yield		**ultimate**		**yield**		**ultimate**	
	P_y, N	**Slip, mm**	**P_u, N**	**Slip, mm**	**P_y, N**	**Peel, mm**	**P_u, N**	**Peel, mm**
FMA2-1	200	0.02	1100	0.12	200	0.1	200	0.1
FMA2-2C	2740	0.007	6170	0.24	1000	0.5	1000	0.5
FRA2-3	480	0.18	675	0.3	1000	0.5	1000	0.5
FMB2-1C	4000	0.01	6000	0.24	1000	0.5	1000	0.5
FMB2-2	1440	0.24	1440	0.24	2000	1	2000	1
FMB2-3	1050	0.35	1050	0.35	2000	1	2000	1

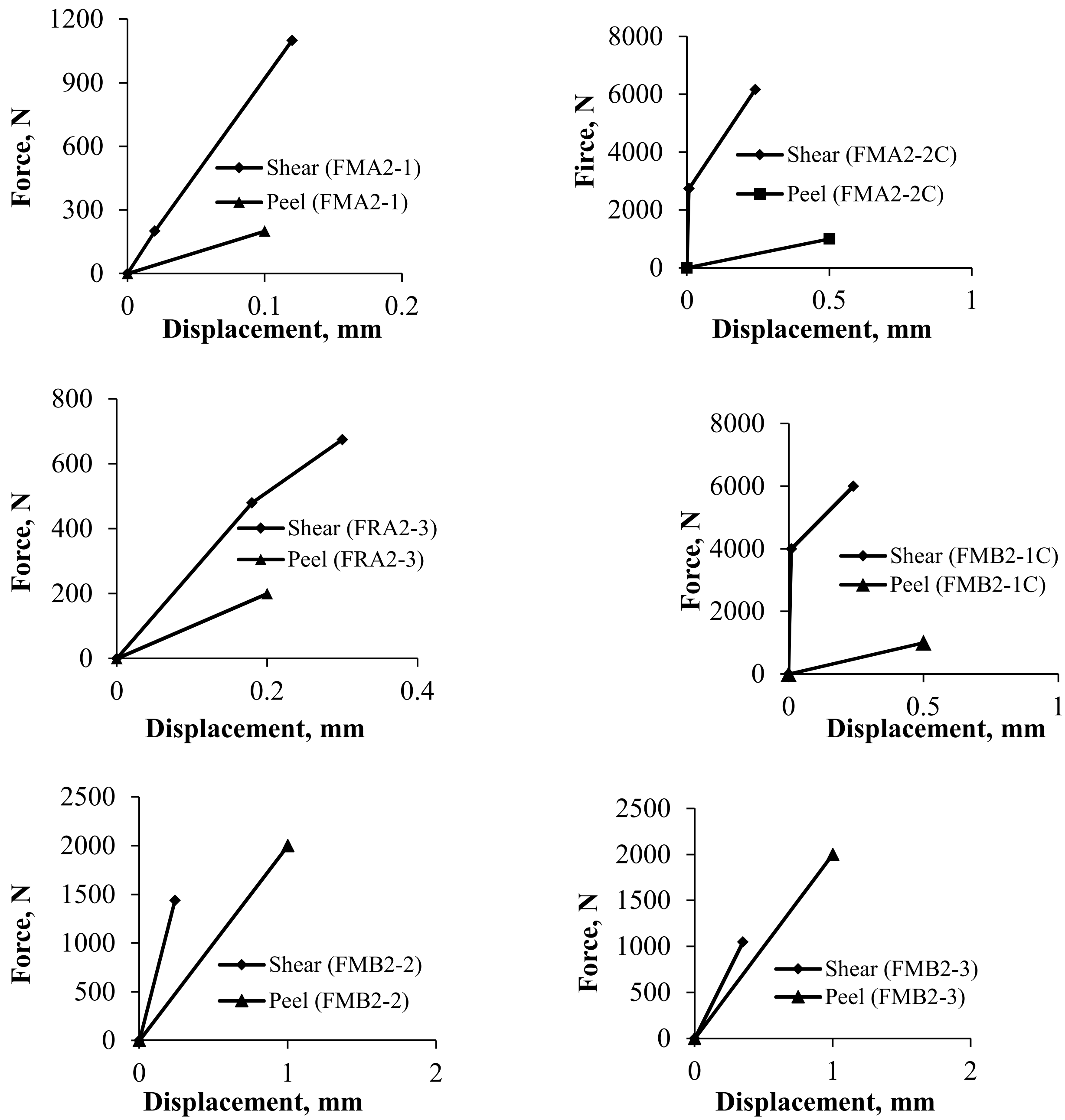

Fig. 19: Interfacial springs properties for slabs from manufacturer A.

Considering slabs with full concrete topping (FMA2-1, FRA2-3, FMB2-2, and FMB2-3), the shear and peel springs behaved in a linear fashion. The length of the concrete topping in those slabs helped distributing the shear stresses over a larger area. When the concrete topping length was reduced for slabs FMA2-2C and FMB2-1C, the shear stresses intensified causing the nonlinear behaviour to become apparent. FEA of the push-off tests and the full-scale tests resulted in maximum interfacial shear stiffnesses of 102 and 297 (N/mm)/mm^2, respectively. The interfacial peel stiffness did not seem to vary between the slabs and was found to be approximately 1.5 (N/mm)/mm^2.

5.2.5 Shear Stress Distribution

The shear stress distribution along the interface between the hollowcore slab and the concrete topping for slab FMA2-1 is shown in Fig. 20. The results were taken for three sections along span: mid-width (x = 610 mm), quarter section (x = 203 mm) and edge section (x = 0). Fig. 20 also shows the interfacial shear stress distribution along the mid-width section at the yielding load, which is the load at which the composite slab stiffness is significantly reduced.

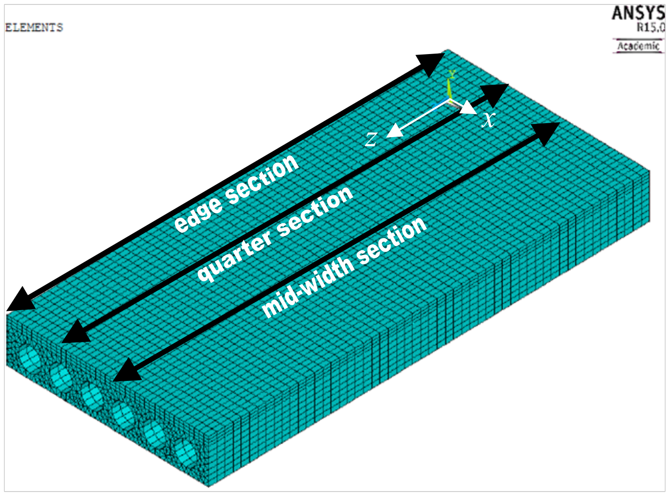

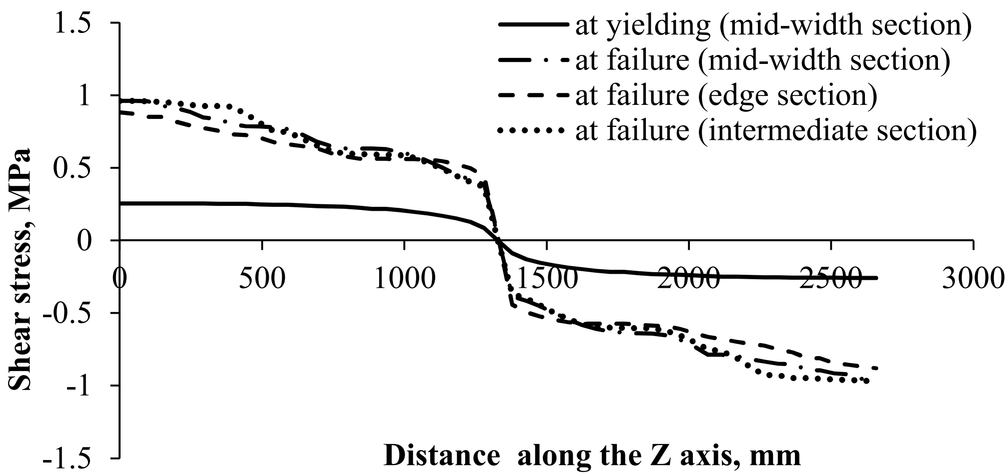

Fig. 20: Interfacial shear stress distribution slab FMA2-1.

Considering the full-scale test setup, where there is only one-point load at mid-span, the maximum interfacial shear stress occurs at the end of the slab where the moment is equal to zero and the vertical shear is at maximum. The shear stress dissipates towards the mid-span section, where the moment is maximum and the vertical shear is equal to zero. The maximum interfacial shear stress sustained by each slab in the full-scale test is presented in Table 6.

With the exception of slabs FRA2-3 and FMB2-3, all tested slabs had sustained relatively higher shear stresses than the 0.55 MPa and 0.7 MPa limits set by the ACI 318-08 (2008) and the CSA A23.3-04 (2004) design standards. The higher stiffness due to the increased thickness for slabs FRA2-3 and FMB2-3 had reduced the intensity of the interfacial shear stress for those slabs.

Table 6: FEA maximum interfacial shear stress results

Slab Label	FMA2-1	FMA2-2C	FRA2-3	FMB2-1C	FMB2-2	FMB2-3
Shear Stress, MPa	0.96	2.0	0.33	3.2	1.85	0.75

6. CONCLUSIONS

Modeling of the push-off and the full-scale tests using the FEA method was conducted in this paper. The FEA showed comparable results with the experimental program conducted by Adawi et al. (2015). This demonstrates that the presented FEA approach and modeling procedures are adequate in capturing the behaviour of composite hollowcore with an acceptable accuracy. A unique modeling technique was used to simulate the staged construction of composite hollowcore slabs. This technique allowed capturing the interface curvature and state of strains before the load was applied. The FEA of the push-off tests provided the nonlinear shear and peel stiffness coefficients of the interface between the hollowcore slab and the concrete topping. Those coefficients were then used as initial values in the FEA of the full-scale tests. The shear stresses were found to reduce the bond strength of the interface layer causing the peel stiffness to significantly reduce. Bond strength evaluated using pull-off tests was found to be uncorrelated with the peel strength.

The use of the full concrete topping reduced the interfacial shear and peel stiffness causing them to behave linearly. When the concrete topping was reduced, the behaviour of the shear and peel changed to be nonlinear and was affected by the interfacial confinement provided by the applied load. This suggests that live loads tend to confine the interface layer in the area where they are applied causing a significant increase in the interfacial shear and peel stiffness. The initial shear stiffness evaluated using FEA of the tested composite hollowcore slabs ranged from 2.2 to 8.3 (N/mm)/mm^2 while the initial peel stiffness was found to be constant at 1.5 (N/mm)/mm^2.

7. ACKNOWLEDGMENTS

The authors would like to acknowledge the enthusiastic guidance, financial support and technical support provided by Mr. Anil Mehta from The Prestressed Group (Windsor, ON).

8. REFERENCES

ACI 318, 2008. Building code requirements for structural concrete (ACI 318-08) and commentary. Michigan, United States: American Concrete Institute.

Adawi A, Youssef MA, Meshaly M, 2015. “Experimental investigation of the composite action between hollowcore slabs with machine-cast finish and concrete topping,” *Engineering Structures*, 91, pp. 1-15.

Adawi A, Youssef MA, Meshaly M., 2014. “Analytical modeling of the interface between lightly roughened hollowcore slabs and cast-in-place concrete topping,” *ASCE J Struct Eng*, V. 141, Issue 04, pp. 119-1 to 119-9.

ANSYS® Academic Research, Release 15.0, 2013, ANSYS, Inc.

ASTM A416/A416 M-02, 2002. Standard Specifications for Steel Strand, Uncoated Seven-Wire for Prestressed Concrete. Pennsylvania, United States: ASTM International.

Balázs, GL, 1992. “Transfer control of prestressing strands,” *PCI journal*, 37(6), 60–71.

Bentz, EC, 2000. “Sectional Analysis of Reinforced Concrete”, *PhD Thesis*, Department of Civil Engineering, University of Toronto.

Bouazaoui L, Perrenot G, Delmas Y and Li A, (2007). “Experimental study of bonded steel concrete composite structures”. *J Constr Steel Res*, 63:1268–78.

Brozzetti J, (2000). “Design development of steel-concrete composite bridges in France”, *J Constr Steel Res*, 55(1–3):229–43.

Celal M., 2011. “Shear Behaviour of Precast/Prestressed Hollow-Core Slabs,” *M.E.Sc. Thesis*, University of Manitoba, Winnipeg, Manitoba, Canada.

Cheng, S and Wang, X, 2010. “Impact of Interaction between Adjacent Webs on the Shear Strength of Prestressed Concrete Hollow-Core Units,” *PCI Journal*, Vol. 55, No. 3, pp. 46-63.

Collins, MP and Mitchell, D, 1991. “Prestressed Concrete Structures,” *Prentice-Hall*, 760 pp.

CSA A23.3, 2004, Design of concrete structures (A23.3-04). Mississauga, ON, Canada: Canadian Standard Association (CSA).

Fabbrocino, G, Manfredi, G, Cosenza, E, (1999). “Non-linear Analysis of composite beams under positive bending”, *Computers and Structures*, 70, 77-89.

Jurkiewiez, B, (2009). “Static and cyclic behaviour of a steel-concrete composite beam with horizontal shear connections”. *J Constr Steel Res*, 65(12):2207–16.

Liang, QQ, Uy, B, Bradford, MA, Ronagh, HR, 2005). “Strength analysis of steel-concrete composite beams in combined bending and shear”. *J Struct Eng*, 131(10):1593–600.

Mones, RM, 2012, “Interfacial Strength Between Prestressed Hollow Core Slabs and Cast-in-Place Concrete Toppings,” *M.E.Sc. Thesis*, University of Massachusetts, Amherst, Massachusetts, United States.

Nie, J, Xiao, Y, Chen, L, (2004). “Experimental studies on shear strength of steel-concrete composite beams”. *J Struct Eng*, 130(8):1206–13.

Ollgard, JG, Slutter, RG, and Fischer, JW (1971). “Shear strength of stud connectors in lightweight and normal concrete.” *AISC Engineering Journal*, 8, 55-64.

Popovics S, 1973. “A Numerical Approach to the Complete Stress-Strain Curve of Concrete,” *Cement and Concrete Research*, Vol. 3, pp. 583-599.

Porasz, A, 1989. “An Investigation of the Stress-Strain Characteristics of High Strength Concrete in Shear,” *M.A.Sc. Thesis*, University of Toronto.

Queiroz, FD, Vellasco, PCGS and Nethercot, DA, 2007. “Finite element modeling of composite beams with full and partial shear connection,” *Journal of Constructional Steel Research*, 63 (2007), pp. 505-521.

Salari, MR, Spacone, E, Benson, P, Frangopol, DM, 1998. “Nonlinear Analysis of Composite Beams with deformable Shear Connectors,” *Journal of Structural Engineering* (ASCE), October 1998, pp. 1148-1158.

Wu, Y, 2015. “Shear Strengthening of Single Web Prestressed Hollow Core Slabs Using Externally Bonded FRP Sheets,” *M.E.Sc. Thesis*. University of Windsor, Windsor, Ontario, Canada.

Luo, Y., Li, A., Kang, Z., (2012). “Parametric study of bonded steel–concrete composite beams by using finite element analysis”. *Engineering Structures*, 34, 40-51.